Q. J. R. Meteorol. Soc. (2004), **??**, pp. 1–20 doi: 10.1256/qj.yy.n

On the use of super compact scheme for spatial differencing in numerical models of the atmosphere

By V. ESFAHANIAN[1]*, S. GHADER[2] and A. R. MOHEBALHOJEH[1]
[1] *University of Tehran, Iran*
[2] *Atmospheric Science & Meteorological Research Centre, Iran*

(Received ??; revised ??)

SUMMARY

The "Super Compact Finite Difference Method" (SCFDM) is applied to spatial differencing of some prototype linear and nonlinear geophysical fluid dynamics problems. An alternative form of the SCFDM relations for spatial derivatives is derived. The sixth-order SCFDM is compared in detail with the conventional fourth-order compact and the second-order centred differencing. For the frequency of linear inertia-gravity waves on different numerical grids (Arakawa's A-E and Randall's Z) related to the Rossby adjustment process, the sixth-order SCFDM shows a substantial improvement on the conventional methods. For the Jacobians involved in vorticity advection by nondivergent flow and in Bolin–Charney balance equation, a general framework, valid for every finite difference method, is derived to present the discrete forms of the Jacobians. It is found that the sixth-order SCFDM provides a noticeably more accurate representation of the wavenumber distribution of the Jacobians, when compared with the conventional methods. The problem of reconstructing the streamfunction field from the vorticity field on a sphere is also considered. For the Rossby–Haurwitz wave, the computation of a normalised global error at different horizontal resolutions in longitude and latitude directions shows that the sixth-order SCFDM can markedly improve on the fourth-order compact. The sixth-order SCFDM is thus proposed as a viable method to improve the accuracy of finite difference models of the atmosphere.

KEYWORDS: Super Compact Finite Difference Numerical Grids Inertia-Gravity Waves Arakawa Jacobian Spherical Geometry

1. INTRODUCTION

A main problem with the spherical harmonic method as the dominant global modeling technique is certainly its rapid increase of computational cost with resolution. There have been various attempts to devise alternative solution techniques able to achieve high accuracy with significantly less computational cost than the spherical harmonic method at very high resolutions. The compact finite difference schemes, introduced as far back as the 1930s, have been found as simple, yet powerful ways of reaching the objectives of high accuracy and low computational cost (Spotz *et al.* 1998, Nihei and Ishii 2003). Compared with the traditional explicit finite difference schemes of the same order, compact schemes have proved to be significantly more accurate with the addeded benefit of using smaller stencil sizes, which can be essential when treating non-periodic boundary conditions.

A recent development in compact schemes has been the introduction of a general procedure to generate highly accurate schemes of arbitrary order with minimal stencil size by Fu Dexun and Ma Yanwen (1995), who called it "Super Compact Finite Difference Method" (SCFDM). The derivation and the application of the method in uniform grid have been presented by Ma Yanwen and Fu Dexun (1996) and by Fu Dexun and Ma Yanwen (2001). In addition, some aspects of the scheme in nonuniform grid have been investigated by Ghader (2000) and Esfahanian *et al.* (2004).

Motivated by the strong performance of the sixth-order SCFDM compared with a traditional explicit and a compact scheme of the same order in simulating

* Corresponding author: Mechanical Engineering Department, University of Tehran, Campus#2, North Karegar Ave., Tehran, Iran. e-mail: evahid@ut.ac.ir

vortex-shock interaction for compressible Navier–Stokes equations (Fu Dexun and Ma Yanwen 2001), this paper is devoted to the assessment of the accuracy of SCFDM in the atmosphere–ocean dynamics context. To this end, we apply the second, fourth, and sixth order SCFDM to spatial differencing of some prototype linear and nonlinear geophysical fluid dynamics problems. In fact, the second and fourth order SCFDM are nothing but the conventional centred and the fourth-order Padé schemes, respectively. To be explicit and avoid any confusion, from now on, we call the schemes: the second-order centred, the fourth-order compact, and the sixth-order SCFDM. The problems examined are (i) linear inertia-gravity wave propagation in f-plane shallow water on different numerical grids (Arakawa's A-E and Randall's Z); (ii) the representation of the dominant nonlinear terms in the vorticity and divergence equations expressed as Jacobians involving only rotational flow; (iii) the solution of the Poisson equation in spherical geometry. Related works can be found in Chang and Shirer (1985), hereafter CS85, and Blayo (2000) on problems (i) and (ii), and in Tolstykh (2002) on problem (iii).

This paper is organised as follows. Section 2 presents the SCFDM relations with the derivation of an alternative form of the SCFDM, making its application to the undertaken problems possible. After presenting the transfer functions of the schemes, Section 3 describes the dispersion relations of the schemes for inertial-gravity waves on f-plane and their comparison with the exact dispersion relation. The numerical approximation of Jacobians involved in vorticity advection by non-divergent flow and in Bolin–Charney balance equation is discussed in section 4, where a general framework valid for every finite-difference method is derived to present the discrete form of the Jacobian operators. The solution of the Poisson equation in spherical geometry to reconstruct the streamfunction field from the vorticity field using SCFDM is presented in sections 5. Finally, the concluding remarks are given in section 6.

2. Super compact method

The super compact finite difference method comprises of a basic equation and a set of auxiliary equations. The basic equation is obtained by truncating the Taylor series which relates a function ϕ to its derivatives,

$$(\alpha\Delta_x^+ + \beta\Delta_x^-)\phi_j = \frac{1}{1!}[\alpha+\beta\sigma_j]\phi_j^{<1>} + \frac{1}{2!}[\alpha-\beta\sigma_j^2]\phi_j^{<2>} + \dots$$
$$+\frac{1}{n!}[\alpha+(-1)^{n+1}\beta\sigma_j^n]\phi_j^{<n>} \qquad (1)$$

where

$$\Delta_x^+\phi_j = \phi_{j+1}-\phi_j, \quad \Delta_x^-\phi_j = \phi_j-\phi_{j-1}, \quad \tilde{h}_j = x_{j+1}-x_j, \quad \tilde{h}_{j-1} = x_j - x_{j-1}$$
$$\sigma_j = \frac{\tilde{h}_{j-1}}{\tilde{h}_j}, \quad \phi_j^{<k>} = \tilde{h}_j^k\left(\frac{\partial^k\phi}{\partial x^k}\right)_j$$

in which α and β are free parameters, Δ_x^+ and Δ_x^- are forward and backward differencing operators, and $\tilde{h}$ denotes grid distance. Note that the formulation can accommodate a nonuniform grid. In Eq. (1), the unknowns are $\phi_j^{<1>}, \phi_j^{<2>}, \dots, \phi_j^{<n>}$. To arrive at a closed system of equations, a set of $(n-1)$

additional independent equations is needed. These auxiliary equations, which are obtained in the same way as the basic equation, read

$$\sigma_{j+1}^{l}\phi_{j+1}^{<l>} - 2\phi_j^{<l>} + \frac{1}{\sigma_j^l}\phi_{j-1}^{<l>} = \frac{1}{1!}(1-\sigma_j)\phi_j^{<l+1>} + \frac{1}{2!}(1+\sigma_j^2)\phi_j^{<l+2>}$$
$$+ \ldots + \frac{1}{(n-l)!}(1+(-1)^{n-l}\sigma_j^{n-l})\phi_j^{<n>} \qquad (l=1,\ldots,n-1). \tag{2}$$

Introducing the n dimensional vectors

$$\mathbf{F} = \left\{\phi^{<1>}, \phi^{<2>}, \ldots, \phi^{<n>}\right\}^{\mathrm{T}}, \qquad \mathbf{E} = \{1, 0, \ldots, 0\}^{\mathrm{T}}$$

where $^{\mathrm{T}}$ denotes transpose, and the $n \times n$ matrices

$$\mathbf{A}(\sigma) = \frac{1}{2}\begin{pmatrix} \frac{\alpha+\beta\sigma}{1!} & \frac{\alpha-\beta\sigma^2}{2!} & \ldots & \frac{\alpha+(-1)^{n+1}\beta\sigma^n}{n!} \\ 0 & \frac{1-\sigma}{1!} & \ldots & \frac{1+(-1)^{n-1}\sigma^{n-1}}{(n-1)!} \\ 0 & 0 & \ldots & \frac{1+(-1)^{n-2}\sigma^{n-2}}{(n-2)!} \\ \ldots & \ldots & \ldots & \ldots \\ 0 & 0 & \ldots & \frac{1-\sigma}{1!} \end{pmatrix}, \quad \mathbf{L}(\sigma) = \begin{pmatrix} 0 & 0 & 0 & 0 & \ldots & 0 \\ \sigma & 0 & 0 & 0 & \ldots & 0 \\ 0 & \sigma^2 & 0 & 0 & \ldots & 0 \\ 0 & 0 & \sigma^3 & 0 & \ldots & 0 \\ \ldots & \ldots & \ldots & \ldots & \ldots & \ldots \\ 0 & 0 & 0 & \ldots & \sigma^{n-1} & 0 \end{pmatrix}$$

one can recast the Eqs. (1) and (2) in a vector form:

$$-\frac{1}{2}\mathbf{L}(\frac{1}{\sigma_j})\ \mathbf{F}_{j-1} + (\mathbf{A}+\mathbf{L})(\sigma_j)\ \mathbf{F}_j - \frac{1}{2}\mathbf{L}(\sigma_{j+1})\ \mathbf{F}_{j+1} = \frac{1}{2}(\alpha\Delta_x^+ + \beta\Delta_x^-)\phi_j\mathbf{E}\ . \tag{3}$$

Here $\phi_j^{<k>}/\tilde{h}_j^k$ approximates $\frac{\partial^k\phi}{\partial x^k}$ with the accuracy of order $n-k+1$. In the case $\sigma_j = 1$, the coefficients in relation (3) do not depend on the coordinate direction and the mesh grid points. At the boundaries, forward and backward relations are used. These relations are derived similar to the centred relations (Ma Yanwen and Fu Dexun 1996; Ghader 2000).

(*a*) *Super compact relations for the odd derivatives*

By choosing $\alpha = \beta = 1$ and $\sigma_j = 1$, the SCFDM relations for odd derivatives are obtained in a uniform grid and Eq. (3) takes the following form

$$-\frac{1}{2}\mathbf{L}\mathbf{F}_{j-1} + (\mathbf{A}+\mathbf{L})\mathbf{F}_j - \frac{1}{2}\mathbf{L}\mathbf{F}_{j+1} = \Delta_x^{\circ}\phi_j\mathbf{E} \tag{4}$$

where $\mathbf{L} = \mathbf{L}(1)$, $\Delta_x^{\circ} = (\Delta_x^+ + \Delta_x^-)/2$ and

$$\mathbf{F} = \begin{pmatrix} \phi^{<1>} \\ \phi^{<3>} \\ \vdots \\ \phi^{<2M-1>} \end{pmatrix}, \quad \mathbf{A} = \begin{pmatrix} \frac{1}{1!} & \frac{1}{3!} & \frac{1}{5!} & \ldots & \frac{1}{(2M-1)!} \\ 0 & \frac{1}{2!} & \frac{1}{4!} & \ldots & \frac{1}{[2(M-1)]!} \\ 0 & 0 & \frac{1}{2!} & \ldots & \frac{1}{[2(M-2)]!} \\ \ldots & \ldots & \ldots & \ldots & \ldots \\ 0 & 0 & 0 & \ldots & \frac{1}{2!} \end{pmatrix}$$

$\mathbf{L}$ and $\mathbf{A}$ are $M \times M$ matrices, $\mathbf{F}$ and $\mathbf{E}$ are M dimensional vectors. The expression $\phi_j^{<2k-1>}/\Delta x^{2k-1}$ approximates $\dfrac{\partial^{2k-1}\phi}{\partial x^{2k-1}}$ with the accuracy of order $2(M-k+1)$.

(*b*) *Super compact relations for the even derivatives*

By choosing $\alpha = -\beta = 1$ and $\sigma_j = 1$, the SCFDM relations for even derivatives are obtained in a uniform grid and Eq. (3) takes the following form

$$-\frac{1}{2}\mathbf{L}\mathbf{S}_{j-1} + (\mathbf{B}+\mathbf{L})\mathbf{S}_j - \frac{1}{2}\mathbf{L}\mathbf{S}_{j+1} = \Delta_x^2\phi_j\mathbf{E} \tag{5}$$

where $\mathbf{L} = \mathbf{L}(1)$, $\Delta_x^2 = \Delta_x^+\Delta_x^- = \Delta_x^-\Delta_x^+$ and

$$\mathbf{S} = \begin{pmatrix} \phi^{<2>} \\ \phi^{<4>} \\ \vdots \\ \phi^{<2M>} \end{pmatrix}, \quad \mathbf{B} = \begin{pmatrix} \frac{1}{2!} & \frac{1}{4!} & \frac{1}{6!} & \dots & \frac{1}{(2M)!} \\ 0 & \frac{1}{2!} & \frac{1}{4!} & \dots & \frac{1}{[2(M-1)]!} \\ 0 & 0 & \frac{1}{2!} & \dots & \frac{1}{[2(M-2)]!} \\ \dots & \dots & \dots & \dots & \dots \\ 0 & 0 & 0 & \dots & \frac{1}{2!} \end{pmatrix}$$

Other matrices and vectors are defined as before. The expression $\phi_j^{<2k>}/\Delta x^{2k}$ approximates $\dfrac{\partial^{2k}\phi}{\partial x^{2k}}$ with the accuracy of order $2(M-k+1)$.

(*c*) *Super compact relations on cell-centred node*

By using the Taylor series for a function on a shifted grid by half (i.e. $\phi_{j\pm\frac{1}{2}}$), the super compact relations on a cell centred node are obtained as follows

$$-\frac{1}{2}\mathbf{L}\mathbf{F}_{j-1} + (\tilde{\mathbf{A}}+\mathbf{L})\mathbf{F}_j - \frac{1}{2}\mathbf{L}\mathbf{F}_{j+1} = \frac{1}{2}(\phi_{j+\frac{1}{2}} - \phi_{j-\frac{1}{2}})\mathbf{E} \tag{6}$$

where

$$\tilde{\mathbf{A}} = \begin{pmatrix} \left(\frac{1}{2}\right)\frac{1}{1!} & \left(\frac{1}{2}\right)^3\frac{1}{3!} & \dots & \left(\frac{1}{2}\right)^{2M-1}\frac{1}{(2M-1)!} \\ 0 & \frac{1}{2!} & \dots & \frac{1}{[2(M-1)]!} \\ 0 & 0 & \frac{1}{2!} & \dots \\ 0 & 0 & \dots & \frac{1}{2!} \end{pmatrix}$$

and other matrices and vectors are defined as before. The expression $\phi_j^{<2k-1>}/\Delta x^{2k-1}$ approximates $\dfrac{\partial^{2k-1}\phi}{\partial x^{2k-1}}$ with the accuracy of order $2(M-k+1)$.

(*d*) *Alternative form of the super compact relations*

In this section a more convenient form of the SCFDM relations (4)-(6) which will be used in the following sections is presented. This alternative form prepares the suitable form of the SCFDM relations for the analytical studies of the next sections.

By using the forward and backward operators which were defined above, the left hand side of Eq. (4) can be written as

$$-\frac{1}{2}\mathbf{L}\mathbf{F}_{j-1}+(\mathbf{A}+\mathbf{L})\mathbf{F}_j-\frac{1}{2}\mathbf{L}\mathbf{F}_{j+1}=\left[\mathbf{A}-\frac{\mathbf{L}}{2}\Delta_x^2\right]\mathbf{F}_j$$

substitution of the above equation into Eq. (4) leads to

$$\left[\mathbf{A}-\frac{\mathbf{L}}{2}\Delta_x^2\right]\mathbf{F}_j=\Delta_x^{\circ}\phi_j\mathbf{E}$$

Finally the alternative form of the Eq. (4) is obtained as

$$\mathbf{F}_j=\left(\frac{\Delta_x^{\circ}}{\mathbf{A}-\frac{\mathbf{L}}{2}\Delta_x^2}\right)\phi_j\mathbf{E}$$

which can be rewritten in the following form

$$\mathbf{F}_j=(\mathbf{Q_o}^{-1}\Delta_x^{\circ})\phi_j\mathbf{E},\quad \mathbf{Q_o}=\mathbf{A}-\frac{\mathbf{L}}{2}\Delta_x^2 \tag{7}$$

Using similar procedure yields the alternative form of the Eq. (5)

$$\mathbf{S}_j=\frac{1}{2}(\mathbf{Q_e}^{-1}\Delta_x^2)\phi_j\mathbf{E},\quad \mathbf{Q_e}=\mathbf{B}-\frac{\mathbf{L}}{2}\Delta_x^2 \tag{8}$$

and the alternative form of the Eq. (6)

$$\mathbf{F}_j=\frac{1}{2}(\mathbf{Q_c}^{-1}\mathbf{E})(\phi_{j+\frac{1}{2}}-\phi_{j-\frac{1}{2}}),\quad \mathbf{Q_c}=\tilde{\mathbf{A}}-\frac{\mathbf{L}}{2}\Delta_x^2 \tag{9}$$

The sixth-order approximations ($M=3$) of the first and second derivatives using Eqs. (7)-(8) are obtained as

$$\phi_j^{<1>}=\left(\frac{10(12+\Delta_x^2)\Delta_x^{\circ}}{120+30\Delta_x^2+\Delta_x^4}\right)\phi_j,\qquad \phi_j^{<2>}=\left(\frac{30(12+\Delta_x^2)\Delta_x^2}{360+60\Delta_x^2+\Delta_x^4}\right)\phi_j \tag{10}$$

and the sixth-order approximation of the first derivative for the cell-centred case yields

$$\phi_j^{<1>}=\left(\frac{320(12+\Delta_x^2)}{1920+240\Delta_x^2+\Delta_x^4}\right)(\phi_{j+\frac{1}{2}}-\phi_{j-\frac{1}{2}})/2 \tag{11}$$

3. Spatial differencing of the linear problems

For the spatial differencing of the linear problems using SCFDM, the linearised shallow water equations on an f-plane are considered. The shallow water equations will be discretized on the well known Arakawa A-E grids (Arakawa

and Lamb 1977), and on the Randall's Z grid (Randall 1994). The grids are defined in Figure 1. We will show that the use of the sixth-order SCFDM to discretize the spatial derivatives leads to better approximation of the dispersion relationship compared with the conventional second and fourth-order schemes. To obtain the discrete dispersion relationships for the A-E grid types we use the general framework derived by Blayo (2000). In addition, we extend this idea to obtain the corresponding framework for the Z grid.

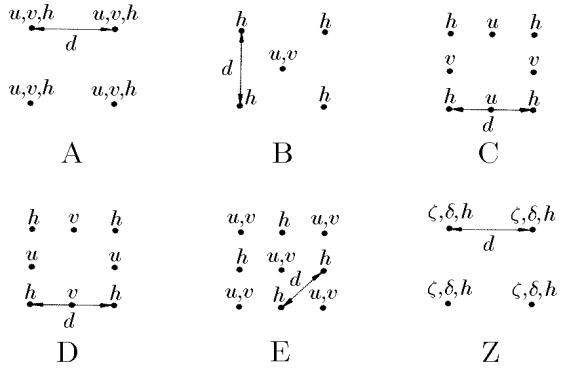

Figure 1. Definition of Arakawa's A-E grids and Randall's Z grid.

(*a*) *Numerical schemes*

In the present study, the sixth-order SCFDM, the fourth-order compact, and the second-order centred schemes are used to discretize the governing equations. We use the following definitions to describe the schemes (Blayo 2000):

1. S_0: an interpolation scheme providing estimates $\phi_{j+\frac{1}{2}}$ of the values ϕ at the midpoints $x_{j+\frac{1}{2}} = (x_j + x_{j+1})/2$.
2. $S_{1/2}$: a scheme providing estimates $\phi'_{j+\frac{1}{2}}$ of the first derivative ϕ' at points $x_{j+\frac{1}{2}}$.
3. S_1: a scheme providing estimates ϕ'_j of the first derivative ϕ' at points x_j.
4. S_2: a scheme providing estimates ϕ''_j of the second derivative ϕ'' at points x_j.

The S_0, $S_{1/2}$, S_1, and S_2 for the three schemes are listed in table 1. To obtain the discrete dispersion relationship for the different grid types (A-E and Z) we need the transfer functions of the schemes listed in table 2. We note that the transfer function, also called response function, T of a scheme S is defined by $S(e^{i\kappa x}) = T(\kappa)e^{i\kappa x}$.

TABLE 1. THE SCHEMES

Scheme	Formulation
Second-order centred	
S_0	$\phi_{j+\frac{1}{2}} = (\phi_j + \phi_{j+1})/2$
$S_{1/2}$	$\phi'_{j+\frac{1}{2}} = (\phi_{j+1} - \phi_j)/d$
S_1	$\phi'_j = (\phi_{j+1} - \phi_{j-1})/2d$
S_2	$\phi''_j = (\phi_{j+1} - 2\phi_j + \phi_{j-1})/d^2$
Compact fourth-order	
S_0	$\frac{1}{6}\phi_{j-\frac{1}{2}} + \phi_{j+\frac{1}{2}} + \frac{1}{6}\phi_{j+\frac{3}{2}} = \frac{2}{3}(\phi_j + \phi_{j+1})$
$S_{1/2}$	$\frac{1}{22}\phi'_{j-\frac{1}{2}} + \phi'_{j+\frac{1}{2}} + \frac{1}{22}\phi'_{j+\frac{3}{2}} = \frac{12}{11}(\phi_{j+1} - \phi_j)/d$
S_1	$\frac{1}{6}\phi'_{j-1} + \frac{2}{3}\phi'_j + \frac{1}{6}\phi'_{j+1} = (\phi_{j+1} - \phi_{j-1})/2d$
S_2	$\frac{1}{12}\phi''_{j-1} + \frac{5}{6}\phi''_j + \frac{1}{12}\phi''_{j+1} = (\phi_{j+1} - 2\phi_j + \phi_{j-1})/d^2$
Super compact sixth-order	
S_0	$\frac{3}{10}\phi_{j-\frac{1}{2}} + \phi_{j+\frac{1}{2}} + \frac{3}{10}\phi_{j+\frac{3}{2}} = \frac{3}{4}(\phi_j + \phi_{j+1}) + \frac{1}{20}(\phi_{j-1} + \phi_{j+2})$
$S_{1/2}$	$\phi'_{j+\frac{1}{2}} = \left(\frac{320(12 + \Delta_x^2)}{1920 + 240\Delta_x^2 + \Delta_x^4}\right)(\phi_{j+1} - \phi_j)/2d$
S_1	$\phi'_j = \left(\frac{10(12 + \Delta_x^2)\Delta_x^\circ}{120 + 30\Delta_x^2 + \Delta_x^4}\right)\phi_j/d$
S_2	$\phi''_j = \left(\frac{30(12 + \Delta_x^2)\Delta_x^2}{360 + 60\Delta_x^2 + \Delta_x^4}\right)\phi_j/d^2$

d is the grid spacing.

(*b*) *The continuous linearised shallow water equations*

The f-plane shallow water equations linearised about a resting basic state are (e.g., Arakawa and Lamb 1977)

$$\begin{aligned} \frac{\partial u}{\partial t} - f_\circ v + g\frac{\partial h}{\partial x} &= 0 \\ \frac{\partial v}{\partial t} + f_\circ u + g\frac{\partial h}{\partial y} &= 0 \\ \frac{\partial h}{\partial t} + H\left(\frac{\partial u}{\partial x} + \frac{\partial v}{\partial y}\right) &= 0 \end{aligned} \tag{12}$$

where H is the constant depth of the water in the basic state, $f_\circ$ the Coriolis parameter and all other symbols have their conventional meanings. An alternative

TABLE 2. The zeroth-order, first-order and second-order transfer functions of the different finite difference methods and the exact operators

Scheme	Transfer function
Exact	
Interpolation	$T_0(\kappa) = 1$
First derivative	$T_1(\kappa) = i\kappa$
Second derivative	$T_2(\kappa) = -\kappa^2$
Second-order centred	
S_0	$T_0(\kappa) = \cos(\kappa d/2)$
$S_{1/2}$	$T_{1/2}(\kappa) = \frac{2i}{d}\sin(\kappa d/2)$
S_1	$T_1(\kappa) = \frac{i}{d}\sin\kappa d$
S_2	$T_2(\kappa) = \frac{-2}{d^2}(1-\cos\kappa d)$
Compact fourth-order	
S_0	$T_0(\kappa) = \frac{4\cos(\kappa d/2)}{3+\cos\kappa d}$
$S_{1/2}$	$T_{1/2}(\kappa) = \frac{2i}{d}\frac{12\sin(\kappa d/2)}{11+\cos\kappa d}$
S_1	$T_1(\kappa) = \frac{i}{d}\frac{3\sin\kappa d}{2+\cos\kappa d}$
S_2	$T_2(\kappa) = \frac{12}{d^2}\frac{\cos\kappa d-1}{\cos\kappa d+5}$
Super compact sixth-order	
S_0	$T_0(\kappa) = \frac{15\cos(\kappa d/2)+\cos(3\kappa d/2)}{10+6\cos\kappa d}$
$S_{1/2}$	$T_{1/2}(\kappa) = \frac{i}{d}\frac{160\sin(3\kappa d/2)+1440\sin(\kappa d/2)}{723+236\cos\kappa d+\cos 2\kappa d}$
S_1	$T_1(\kappa) = \frac{i}{d}\frac{10\sin 2\kappa d+100\sin\kappa d}{66+52\cos\kappa d+2\cos 2\kappa d}$
S_2	$T_2(\kappa) = \frac{1}{d^2}\frac{30\cos 2\kappa d+240\cos\kappa d-270}{\cos 2\kappa d+56\cos\kappa d+123}$

form of (12) in terms of vorticity ζ and divergence δ is

$$\begin{aligned} &\frac{\partial\delta}{\partial t} - f_\circ\zeta + g\left(\frac{\partial^2 h}{\partial x^2}+\frac{\partial^2 h}{\partial y^2}\right) = 0 \\ &\frac{\partial\zeta}{\partial t} + f_\circ\delta = 0 \\ &\frac{\partial h}{\partial t} + H\delta = 0 \end{aligned} \tag{13}$$

By assuming wave solutions, the following dispersion relation is obtained:

$$\left(\frac{\omega}{f_\circ}\right)^2 = 1+\lambda^2(\kappa^2+\ell^2) \tag{14}$$

where ω is the frequency, $\lambda = \sqrt{gH}/f_\circ$ is the Rossby radius of deformation, and κ and ℓ are the wavenumbers in the x and y directions, respectively.

(c) *Discrete dispersion relationship*

To represent the discrete dispersion relationships for the inertia-gravity waves on Arakawa A-E grids, the generic expressions of the discrete dispersion relationships derived by Blayo (2000) are used. This idea, here, can be extended in a similar way to obtain the discrete dispersion relation for the Z grid. Therefore, the discrete dispersion relations for the inertia-gravity waves on the A-E and Z grids will be

$$
\begin{aligned}
\text{A}: &\quad \left(\frac{\omega}{f_\circ}\right)^2 = 1 - \lambda^2 \left[T_1^2(\kappa) + T_1^2(\ell)\right] \\
\text{B}: &\quad \left(\frac{\omega}{f_\circ}\right)^2 = 1 - \lambda^2 \left[T_{1/2}^2(\kappa)\, T_0^2(\ell) + T_{1/2}^2(\ell)\, T_0^2(\kappa)\right] \\
\text{C}: &\quad \left(\frac{\omega}{f_\circ}\right)^2 = T_0^2(\kappa)\, T_0^2(\ell) - \lambda^2 \left[T_{1/2}^2(\kappa) + T_{1/2}^2(\ell)\right] \\
\text{D}: &\quad \left(\frac{\omega}{f_\circ}\right)^2 = T_0^2(\kappa)\, T_0^2(\ell) - \lambda^2 \left[T_1^2(\kappa)\, T_0^2(\ell) + T_1^2(\ell)\, T_0^2(\kappa)\right] \\
\text{E}: &\quad \left(\frac{\omega}{f_\circ}\right)^2 = 1 - \lambda^2 \left[T_{1/2}^2(\kappa) + T_{1/2}^2(\ell)\right] \\
\text{Z}: &\quad \left(\frac{\omega}{f_\circ}\right)^2 = 1 - \lambda^2 \left[T_2(\kappa) + T_2(\ell)\right]
\end{aligned}
\tag{15}
$$

The discrete dispersion relations for our second, fourth, and sixth-order schemes applied to the A-E and Z grids will be found using the transfer functions of these methods, given in table 2.

The results of the discrete relations of the different methods on the numerical A-E and Z grids are presented for a resolved ($\lambda/d = 2$) and for an under-resolved ($\lambda/d = 1/2$) cases, and are compared with the exact continuous relation. The significance of these choices of λ/d has been discussed by Randall (1994). Figure 2 shows the exact nondimensional frequency $\omega/f_\circ$ and the sixth-order SCFDM representation of the discrete relation as a function of κd and ℓd for the case $\lambda/d = 2$, on the different numerical grids. The region where the discrete and exact dispersion relationships coincide, is at the lower left-hand corner. Comparing these results obtained from the sixth-order SCFDM, with the second-order centred (Randall 1994, Dukowicz 1995) and the fourth-order compact (performed by present authors) shows a clear improvement in the coincide region. Since it may not be easy to compare the accuracy of the discretizations obtained by different methods, the relative error of each method on different grids is plotted. The relative error is defined as $|\omega_\mathrm{e} - \omega_\mathrm{n}|/|\omega_\mathrm{e}|$, where ω_e is the exact frequency obtained from Eq. (14) and ω_n is the grid frequency which is computed for different methods on A-E and Z grids. Figure 3 presents the 10% error contour for the second-order centred on different grids for the resolved and under-resolved cases ($\lambda/d = 2, 1/2$). Figures 4 and 5 show the 10% error contour for the fourth-order compact and the sixth-order SCFDM, respectively. It can be seen that the sixth-order SCFDM leads to a very clear increase in the accuracy of the frequency of inertia-gravity waves. For each of the three schemes, the best results come from the C grid for the resolved case and the B grid for the under-resolved case when the Arakawa grids are used, but the Z grid gives the best results for both cases.

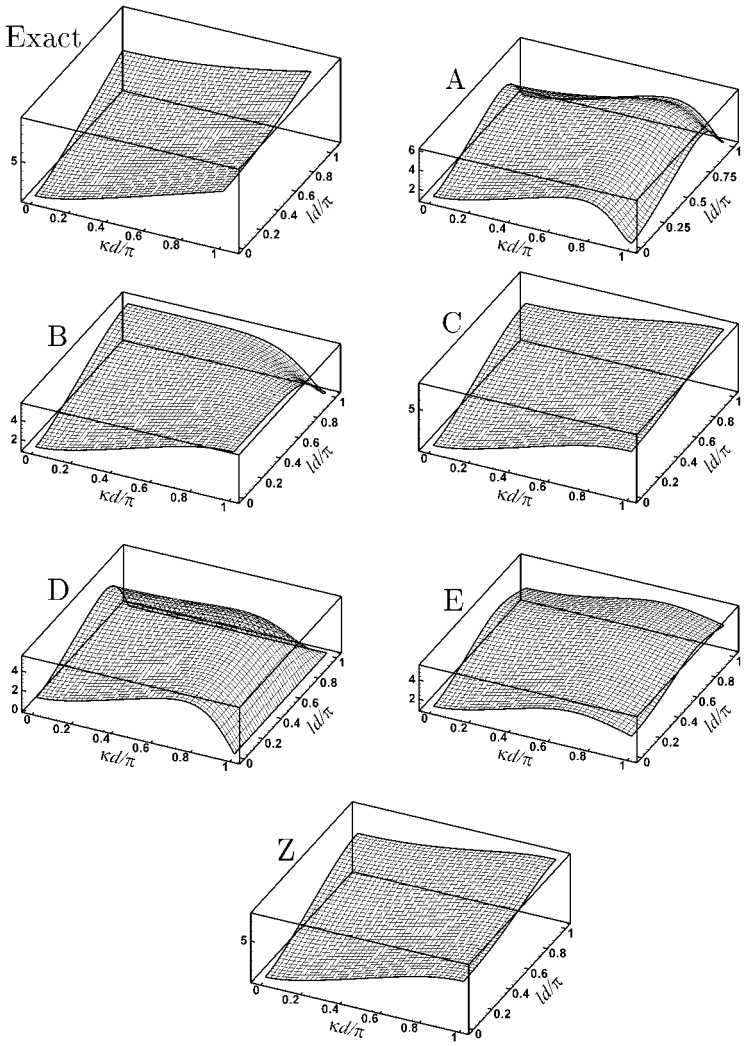

Figure 2. The exact and the sixth-order super compact representation of the nondimensional frequency $\omega/f_\circ$ for inertia-gravity waves with $\lambda/d = 2$. The horizontal coordinates in the plots are κd and ℓd, respectively, except for the E grid for which $\sqrt{2}\kappa d$ and $\sqrt{2}\ell d$ are used.

4. Spatial differencing of some prototype nonlinear problems

Let us see how the nonlinearity is affected by spatial differencing. To this end, we study the two Jacobians appearing in the vorticity and divergence equations as the dominant nonlinear terms. The Jacobians are $J(\psi, \zeta)$ and $J(u_\psi, v_\psi)$, where ψ is the streamfunction, $u_\psi = -\partial\psi/\partial y$, $v = \partial\psi/\partial x$, and $J(X, Y) = \partial X/\partial x \partial Y/\partial y - \partial X/\partial y \partial Y/\partial x$ for any two arbitrary quantities X and Y. Physically speaking, $J(\psi, \zeta)$ represents vorticity advection by nondivergent flow, and apart from a factor 2 dropped for convenience, $J(u_\psi, v_\psi)$ represents the nonlinear term in Bolin–Charney balance equation. In what follows, we assume that the streamfunction and vorticity are on an unstaggered grid. The different, though identical in continuous case, forms of the Jacobian operator for vorticity

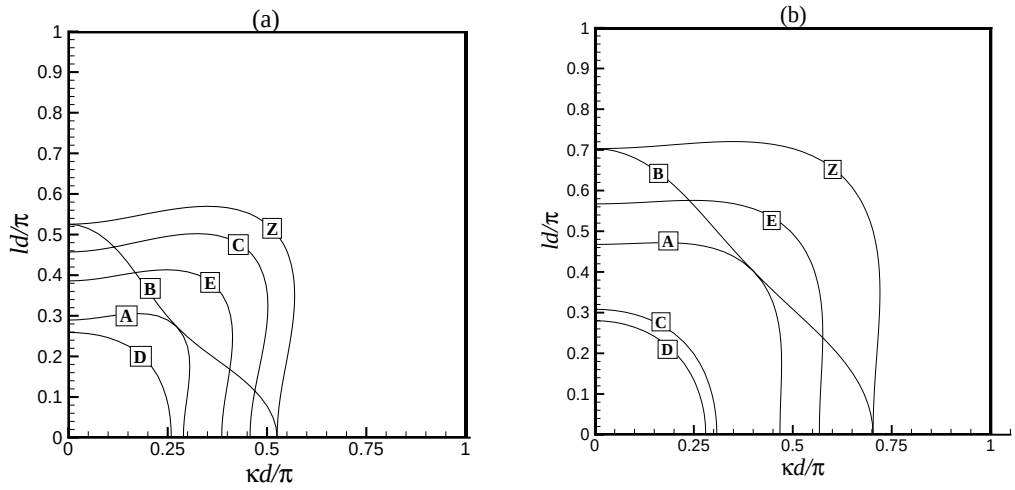

Figure 3. Contour lines of 10% error in frequency for the dispersion relationship of the inertia-gravity wave on A-E and Z grids obtained from the second-order method, (a) $\lambda/d = 2$ and (b) $\lambda/d = 1/2$.

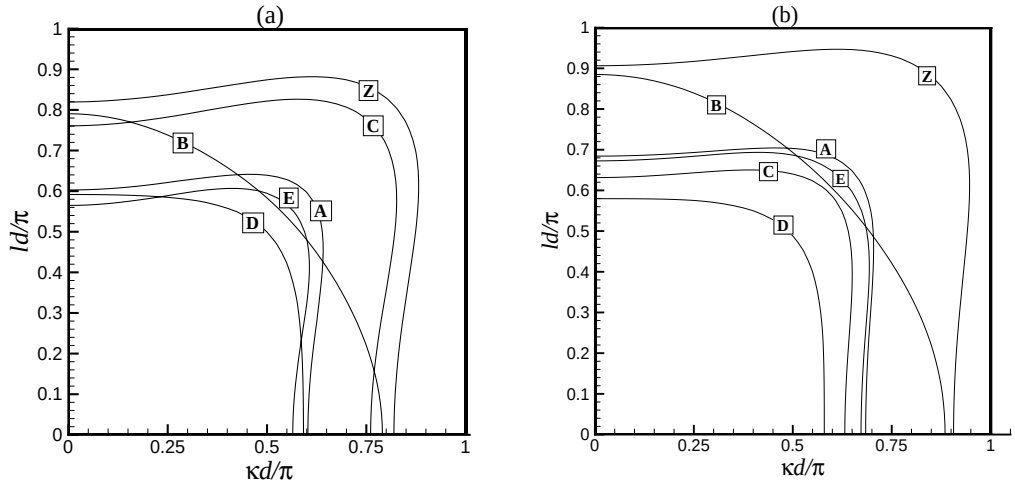

Figure 4. Contour lines of 10% error in frequency for the dispersion relationship of the inertia-gravity wave on A-E and Z grids obtained from the fourth-order compact method, (a) $\lambda/d = 2$ and (b) $\lambda/d = 1/2$.

advection read (Lilly 1965; Haltiner and Williams 1980):

$$\begin{aligned} J_1(\psi,\zeta) &= \frac{\partial\psi}{\partial x}\frac{\partial\zeta}{\partial y} - \frac{\partial\psi}{\partial y}\frac{\partial\zeta}{\partial x} \\ J_2(\psi,\zeta) &= \frac{\partial}{\partial x}\left(\psi\frac{\partial\zeta}{\partial y}\right) - \frac{\partial}{\partial y}\left(\psi\frac{\partial\zeta}{\partial x}\right) \\ J_3(\psi,\zeta) &= \frac{\partial}{\partial y}\left(\zeta\frac{\partial\psi}{\partial x}\right) - \frac{\partial}{\partial x}\left(\zeta\frac{\partial\psi}{\partial y}\right) \\ J_{\rm A}(\psi,\zeta) &= \frac{1}{3}\left(J_1 + J_2 + J_3\right) \end{aligned} \tag{16}$$

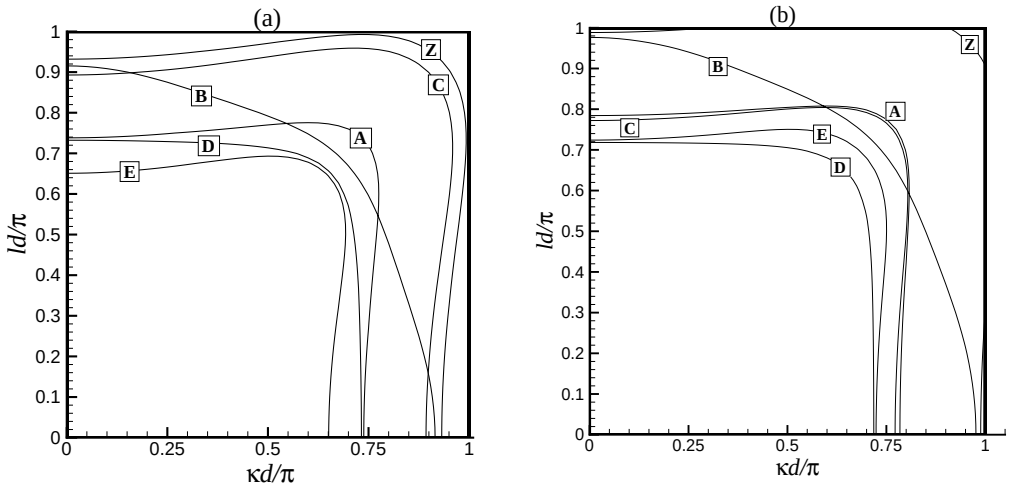

Figure 5. Contour lines of 10% error in frequency for the dispersion relationship of the inertia-gravity wave on A-E and Z grids obtained from the sixth-order super compact method, (a) $\lambda/d = 2$ and (b) $\lambda/d = 1/2$.

where

$$\zeta = \nabla^2 \psi = \frac{\partial^2 \psi}{\partial x^2} + \frac{\partial^2 \psi}{\partial y^2} \tag{17}$$

and J_{A} denotes the Arakawa Jacobian. It should be emphasized here that the Jacobian operators (16) are different when discretized by numerical methods.

Following CS85 and Lorenz (1960), for a doubly periodic domain, the continuous ψ is expanded in a complex Fourier series with vector wavenumber $\mathbf{M} = m\mathbf{x} + n\mathbf{y}$ as

$$\psi = \sum_{\mathbf{M}} A_{\mathbf{M}} \exp[\mathrm{i}(\mathbf{M} \cdot \mathbf{R})] \equiv \sum_{\mathbf{M}} \psi_{\mathbf{M}} \tag{18}$$

in which $\mathbf{x}$ and $\mathbf{y}$ are the unit vectors in the x and y directions, respectively, $\mathrm{i} = \sqrt{-1}$, $\mathbf{R} = x\mathbf{x} + y\mathbf{y}$ and the summation is over a finite set of integral wavenumbers m and n. From Eqs. (17) and (18), u_ψ, v_ψ, and ζ can be written as

$$u_\psi = -\sum_{\mathbf{M}} \mathrm{i} n A_{\mathbf{M}} \exp[\mathrm{i}(\mathbf{M} \cdot \mathbf{R})]$$

$$v_\psi = \sum_{\mathbf{M}} \mathrm{i} m A_{\mathbf{M}} \exp[\mathrm{i}(\mathbf{M} \cdot \mathbf{R})]$$

$$\zeta = -\sum_{\mathbf{M}} |\mathbf{M}|^2 A_{\mathbf{M}} \exp[\mathrm{i}(\mathbf{M} \cdot \mathbf{R})] = -\sum_{\mathbf{M}} |\mathbf{M}|^2 \psi_{\mathbf{M}} \tag{19}$$

Symmetric forms for $J(\psi, \zeta)$ (Lilly 1965) and $J(u_\psi, v_\psi)$ can be obtained analytically, which read

$$J(\psi, \zeta) = \frac{1}{2} \sum_{\mathbf{M}'} \sum_{\mathbf{M}''} (\mathbf{k} \cdot \mathbf{M}' \times \mathbf{M}'') \left(|\mathbf{M}''|^2 - |\mathbf{M}'|^2 \right) \psi_{\mathbf{M}'} \psi_{\mathbf{M}''} \tag{20}$$

$$J(u_\psi, v_\psi) = \frac{1}{2} \sum_{\mathbf{M}'} \sum_{\mathbf{M}''} [\mathbf{k} \cdot (\mathbf{M}' \times \mathbf{M}'')]^2 \psi_{\mathbf{M}'} \psi_{\mathbf{M}''} \tag{21}$$

where the unit vector $\mathbf{k} = \mathbf{x} \times \mathbf{y}$. Here a general framework, valid for every finite difference scheme, is derived to express the discrete form for each of the Jacobian operators. For the sake of clarity, we differentiate the grid-base discrete quantities by a tilde over their continuous counterparts. Assuming the following expansion for the discrete streamfunction at the grid point i, j,

$$\tilde{\psi}_{i,j} = \sum_{\mathbf{M}} A_{\mathbf{M}} \exp[\mathrm{i}(\mathbf{M} \cdot \mathbf{R}_{i,j})] \equiv \sum_{\mathbf{M}} \tilde{\psi}_{\mathbf{M}} \ ,$$

the discrete u_ψ, v_ψ, and ζ can then be expressed as

$$(\tilde{u}_\psi)_{i,j} = -\sum_{\mathbf{M}} \mathrm{i}\,(\mathbf{y} \cdot \mathcal{P}(\mathbf{M}))\,\tilde{\psi}_{\mathbf{M}} \ ,$$

$$(\tilde{v}_\psi)_{i,j} = \sum_{\mathbf{M}} \mathrm{i}\,(\mathbf{x} \cdot \mathcal{P}(\mathbf{M}))\,\tilde{\psi}_{\mathbf{M}} \ ,$$

$$\tilde{\zeta}_{i,j} = -\sum_{\mathbf{M}} \mathcal{T}(\mathbf{M})\tilde{\psi}_{\mathbf{M}} \ .$$

Here for convenience, we have defined the vector function $\mathcal{P}(\mathbf{M})$ and the scalar function $\mathcal{T}(\mathbf{M})$ related to the transfer functions of the first and second derivatives, respectively,

$$\begin{aligned} \mathcal{P}(\mathbf{M}) &= -\mathrm{i}[T_1(m)\mathbf{x} + T_1(n)\mathbf{y}] \ , \\ \mathcal{T}(\mathbf{M}) &= -[T_2(m) + T_2(n)] \ . \end{aligned}$$

By substituting the above expressions for $\tilde{\psi}$, $\tilde{u}_\psi$, $\tilde{v}_\psi$, and $\tilde{\zeta}$ in the different Jacobian operators (16), their discrete versions are obtained

$$\begin{aligned} \tilde{J}_1(\tilde{\psi}, \tilde{\zeta}) &= \frac{1}{2} \sum_{\mathbf{M}'} \sum_{\mathbf{M}''} \mathbf{k} \cdot \{\mathcal{P}(\mathbf{M}') \times \mathcal{P}(\mathbf{M}'')\}\,[\mathcal{T}(\mathbf{M}'') - \mathcal{T}(\mathbf{M}')]\tilde{\psi}_{\mathbf{M}'}\tilde{\psi}_{\mathbf{M}''} \\ \tilde{J}_2(\tilde{\psi}, \tilde{\zeta}) &= \frac{1}{2} \sum_{\mathbf{M}'} \sum_{\mathbf{M}''} \mathbf{k} \cdot \mathcal{P}[(\mathbf{M}' + \mathbf{M}'')] \times \{\mathcal{P}(\mathbf{M}'')\mathcal{T}(\mathbf{M}'') + \mathcal{P}(\mathbf{M}')\mathcal{T}(\mathbf{M}')\}\,\tilde{\psi}_{\mathbf{M}'}\tilde{\psi}_{\mathbf{M}''} \\ \tilde{J}_3(\tilde{\psi}, \tilde{\zeta}) &= -\frac{1}{2} \sum_{\mathbf{M}'} \sum_{\mathbf{M}''} \mathbf{k} \cdot \mathcal{P}[(\mathbf{M}' + \mathbf{M}'')] \times \{\mathcal{P}(\mathbf{M}'')\mathcal{T}(\mathbf{M}') + \mathcal{P}(\mathbf{M}')\mathcal{T}(\mathbf{M}'')\}\,\tilde{\psi}_{\mathbf{M}'}\tilde{\psi}_{\mathbf{M}''} \\ \tilde{J}_{\mathrm{A}}(\tilde{\psi}, \tilde{\zeta}) &= \frac{1}{6} \sum_{\mathbf{M}'} \sum_{\mathbf{M}''} \mathbf{k} \cdot \{\mathcal{P}(\mathbf{M}') \times \mathcal{P}(\mathbf{M}'') + \mathcal{P}[(\mathbf{M}' + \mathbf{M}'')] \times [\mathcal{P}(\mathbf{M}'') - \mathcal{P}(\mathbf{M}')]\} \\ &\qquad [\mathcal{T}(\mathbf{M}'') - \mathcal{T}(\mathbf{M}')]\tilde{\psi}_{\mathbf{M}'}\tilde{\psi}_{\mathbf{M}''} \ . \end{aligned} \tag{22}$$

Similarly, the discrete versions of $J(u_\psi, v_\psi)$ can be found. For the sake of brevity, we only give the expression for $J_1(u_\psi, v_\psi)$ and $J_{\mathrm{A}}(u_\psi, v_\psi)$, which reads

$$\tilde{J}_1(\tilde{u}_\psi, \tilde{v}_\psi) = \frac{1}{2} \sum_{\mathbf{M}'} \sum_{\mathbf{M}''} \{\mathbf{k} \cdot [\mathcal{P}(\mathbf{M}') \times \mathcal{P}(\mathbf{M}'')]\}^2 \tilde{\psi}_{\mathbf{M}'}\tilde{\psi}_{\mathbf{M}''} \tag{23}$$

$$\begin{aligned} \tilde{J}_{\mathrm{A}}(\tilde{u}_\psi, \tilde{v}_\psi) &= \frac{1}{6} \sum_{\mathbf{M}'} \sum_{\mathbf{M}''} \{(\mathbf{k} \cdot [\mathcal{P}(\mathbf{M}') \times \mathcal{P}(\mathbf{M}'')])(\mathbf{k} \cdot [\mathcal{P}(\mathbf{M}') \times \mathcal{P}(\mathbf{M}'')] + \\ &\qquad \mathbf{k} \cdot [\mathcal{P}(\mathbf{M}') - \mathcal{P}(\mathbf{M}'')] \times \mathcal{P}(\mathbf{M}' + \mathbf{M}''))\}\tilde{\psi}_{\mathbf{M}'}\tilde{\psi}_{\mathbf{M}''} \ . \end{aligned} \tag{24}$$

Now it remains to find the functions $\mathcal{P}$ and $\mathcal{T}$ for the numerical schemes studied, which are easily obtained by using the first and second order transfer

functions given in table 2. These functions are

$$\mathcal{P}(\mathbf{M}) = \frac{\sin(md)}{d}\mathbf{x} + \frac{\sin(nd)}{d}\mathbf{y}, \quad \mathcal{T}(\mathbf{M}) = \frac{\sin^2(md/2)}{(d/2)^2} + \frac{\sin^2(nd/2)}{(d/2)^2}$$

for the second-order centred, the same as the results by Lilly (1965),

$$\mathcal{P}(\mathbf{M}) = \frac{3\sin(md)}{d[2+\cos(md)]}\mathbf{x} + \frac{3\sin(nd)}{d[2+\cos(nd)]}\mathbf{y}, \ \mathcal{T}(\mathbf{M}) = \frac{12[1-\cos(md)]}{d^2[5+\cos(md)]} + \frac{12[1-\cos(nd)]}{d^2[5+\cos(nd)]}$$

for the compact fourth-order as derived by CS85, and

$$\begin{aligned}
\mathcal{P}(\mathbf{M}) &= \frac{10\sin(2md)+100\sin(md)}{d[66+52\cos(md)+2\cos(2md)]}\mathbf{x} + \frac{10\sin(2nd)+100\sin(nd)}{d[66+52\cos(nd)+2\cos(2nd)]}\mathbf{y} \\
\mathcal{T}(\mathbf{M}) &= -\frac{1}{d^2}\left\{\frac{30\cos(2md)+240\cos(md)-270}{\cos(2md)+56\cos(md)+123} + \frac{30\cos(2nd)+240\cos(nd)-270}{\cos(2nd)+56\cos(nd)+123}\right\}
\end{aligned}$$

for the sixth-order SCFDM.

A detailed account of the properties of the Jacobian operators $\tilde{J}_1$, $\tilde{J}_2$, $\tilde{J}_3$, and $\tilde{J}_7$ for the vorticity advection are given in CS85. A brief account following CS85 is given here. The numerical errors in the discrete Jacobians come from two sources, (i) the *amplitude errors* associated with the finite difference approximations for the first and the second derivatives and (ii) the *coupling errors* associated with the nonlinear interactions. The coupling errors involve waves of all wavelengths and are distinct form aliasing errors. The magnitudes of the coupling errors in the approximations of J_2 and J_3 are equal but of opposite signs. The coupling errors do not appear in J_1 and thus in J_A. For J_1 the aliasing errors will amplify. Due to the very accurate representation of energy exchanges among different waves, the Arakawa Jacobian is preferred for the discretization of the vorticity advection expressed in Jacobian. It is interesting to note that the $\tilde{J}_2$, $\tilde{J}_3$, and $\tilde{J}_7$ counterparts of $\tilde{J}_1$ given in Eq. (23) for $J(u_\psi, v_\psi)$ share the same properties with $J(\psi, \zeta)$ outlined above as regards the coupling errors. It seems that the discrete counterparts of $J(\psi, \zeta)$ and $J(u_\psi, v_\psi)$ hold the same wave-wave interaction properties.

In this paper, only the results for the amplitude errors of $\tilde{J}_A(\tilde{\psi}, \tilde{\zeta})$ and $\tilde{J}_1(\tilde{u}_\psi, \tilde{v}_\psi)$ are presented. Like CS85, we assume that ψ is composed of two components having different wanenumbers m_1 and m_2 in the x-direction and wavenumber n in the y-direction

$$\psi = A_{m_1,n}\exp[\mathrm{i}(m_1 x + ny)] + A_{m_2,n}\exp[\mathrm{i}(m_2 x + ny)] \tag{25}$$

By substituting Eq. (25) into Eq. (20) and Eq. (21), respectively, the exact analytical expressions for the continuous Jacobians are obtained as

$$J(\psi,\zeta) = -n(m_2 - m_1)(m_2^2 - m_1^2)A_{m_1,n}A_{m_2,n}\exp\{\mathrm{i}[(m_1+m_2)x + 2ny]\} \tag{26}$$

$$J(u_\psi, v_\psi) = n^2(m_1 - m_2)^2 A_{m_1,n}A_{m_2,n}\exp\{\mathrm{i}[(m_1+m_2)x + 2ny]\} \tag{27}$$

Similarly, making use of the functions $\mathcal{P}$ and $\mathcal{T}$ for different numerical methods, and substituting Eq. (25) into Eq. (22) and Eq. (23) give us the discrete, approximate expression for each Jacobian and each numerical method. For $\tilde{J}_1$ and $\tilde{J}_A$, consistent with the exact results the nonlinear interaction between the two waves (m_1, n) and (m_2, n) will transfer energy solely into the wave $(m_1 + m_2, 2n)$.

To evaluate the exact and approximate Jacobians, it is appropriate to make a physically meaningful model for the amplitude $A_{m,n}$. To this end, we freely borrow from the numerical results of Yuan and Hamilton (1994), hereafter YH94, for the forced-dissipative f-plane shallow water turbulence. We assume the energy spectrum presented in Fig. 6 for the potentio-vortical component of the flow, which is a slight idealisation of that given in Fig. 4 of YH94. To recover the amplitude for streamfunction, we use quasigeostrophic relations in the potentio-vortical energy E in spectral space given by YH94 in their Eq. 2.23,

$$E = \frac{1}{2} H (m^2 + n^2 + \frac{1}{\lambda^2}) A_{m,n}^2 \tag{28}$$

and obtain $A_{m,n} = \left(2E/(H(m^2 + n^2 + 1/\lambda^2))\right)^{1/2}$. Adapting the dimensional parameters used by YH94 to a 2π doubly-periodic domain for convenience, we take $H = 1$, $\lambda = 0.3$, $n = 1$, and $m_1, m_2 = 1, 2, \ldots, 64$. Figure 7 presents the analytical Jacobians (26) and (27) against the wavenumbers m_1 and m_2. The contours show the exact values of the Jacobians, more precisely the factors in front of $\exp\{\mathrm{i}[(m_1 + m_2)x + 2ny]\}$ in (26) and (27). It can be seen that large values for the Jacobians will appear when the difference in the wavenumbers between the two waves is very large and the wavenumbers are not too large. Figure 7 also shows a zone of weak interactions around the line $m_1 = m_2$, the size of which decreases at the lower left-hand corner of the figure. Figure 8 presents the 5% and

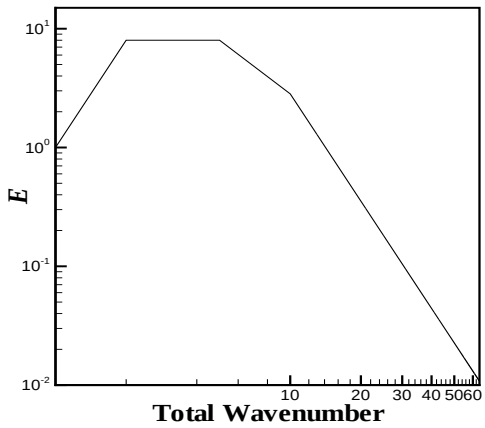

Figure 6. The potentio-vortical energy spectrum used to model the wavenumber distribution of the amplitude of ψ.

20% relative errors for $\tilde{J}_{\mathrm{A}}(\tilde{\psi}, \tilde{\zeta})$ and $\tilde{J}_1(\tilde{u}_\psi, \tilde{v}_\psi)$ and the three numerical schemes. Notice that the error increases from small to large values of m_1 and m_2 almost isotropically, except for a reduction at large values of the wavenumbers at the upper right-hand corner for $\tilde{J}_1(\tilde{u}_\psi, \tilde{v}_\psi)$. It is clear that the fourth-order compact method gives a significant improvement on the second-order centred. Further, the sixth-order SCFDM enjoys a noticeably larger region with relative error less than both 5% and 20% compared with the fourth-order compact. It is expected that the use of sixth-order SCFDM will further improve the representation of wave-wave interactions. Global measures for the error in the spectral space of m_1 and m_2 are given in table 3 for the two Jacobians using 64 and 128 waves. The

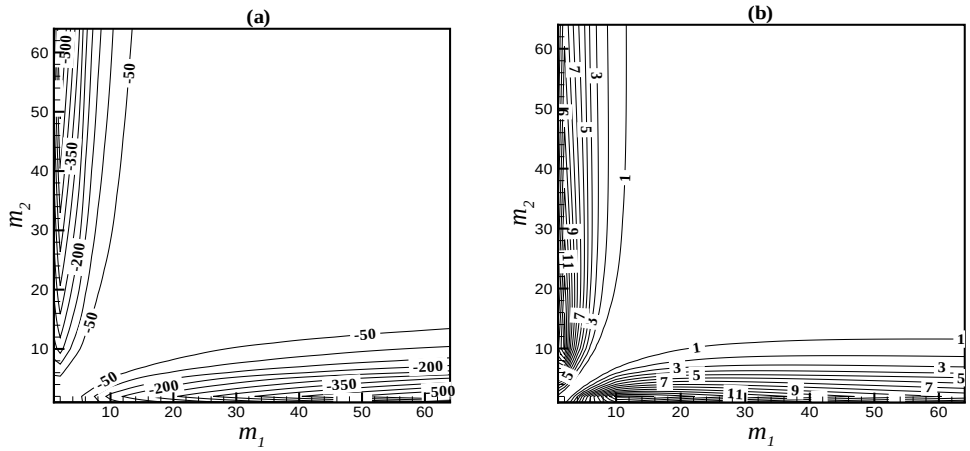

Figure 7. The distribution of exact values of (a) $J(\psi, \zeta)$ and (b) $J(u_\psi, v_\psi)$ obtained analytically from (26) and (27). The contours represent the amplitudes of the wave $(m_1 + m_2, 2n)$.

global error, a normalised l_2 norm, is defined by

$$l_2(J) = \frac{\left\{ I\left(|\tilde{J}(m_1, m_2) - J(m_1, m_2)|^2 \right) \right\}^{1/2}}{\left\{ I\left(|J(m_1, m_2|^2 \right) \right\}^{1/2}} \tag{29}$$

where

$$I(J) = \sum_{m_1=1}^{N_m} \sum_{m_2=1}^{N_m} J_{m_1, m_2} \tag{30}$$

and N_m is the number of waves used. Compared with the fourth-order compact, a nearly 25% reduction in error is observed for the sixth-order SCFDM.

TABLE 3. Global error measures for the second, fourth, and sixth order approximations to $J(\psi, \zeta)$ and $J(u_\psi, v_\psi)$ using 64 and 128 waves.

	$J(\psi, \zeta)$		$J(u_\psi, v_\psi)$	
Method	$N_m = 64$	$N_m = 128$	$N_m = 64$	$N_m = 128$
Second-order centred	0.80280	0.76987	0.66615	0.57489
Compact fourth-order	0.57361	0.54073	0.42118	0.35456
Super compact sixth-order	0.46415	0.43213	0.33165	0.27698

5. Spherical geometry

In this section, the problem of reconstruction of the streamfunction field from the vorticity on the sphere is considered. A well-known analytical solution is used to compare the results of the three schemes. For the analytical case the Rossby–Haurwitz wave, which is one of the standard tests proposed by Williamson *et al.* (1992), is used. For the Rossby–Haurwitz wave the initial velocity field is nondivergent and given by the streamfunction

$$\psi = -a^2 \nu \sin\varphi + a^2 K \cos^R \varphi \sin\varphi \cos R\lambda$$

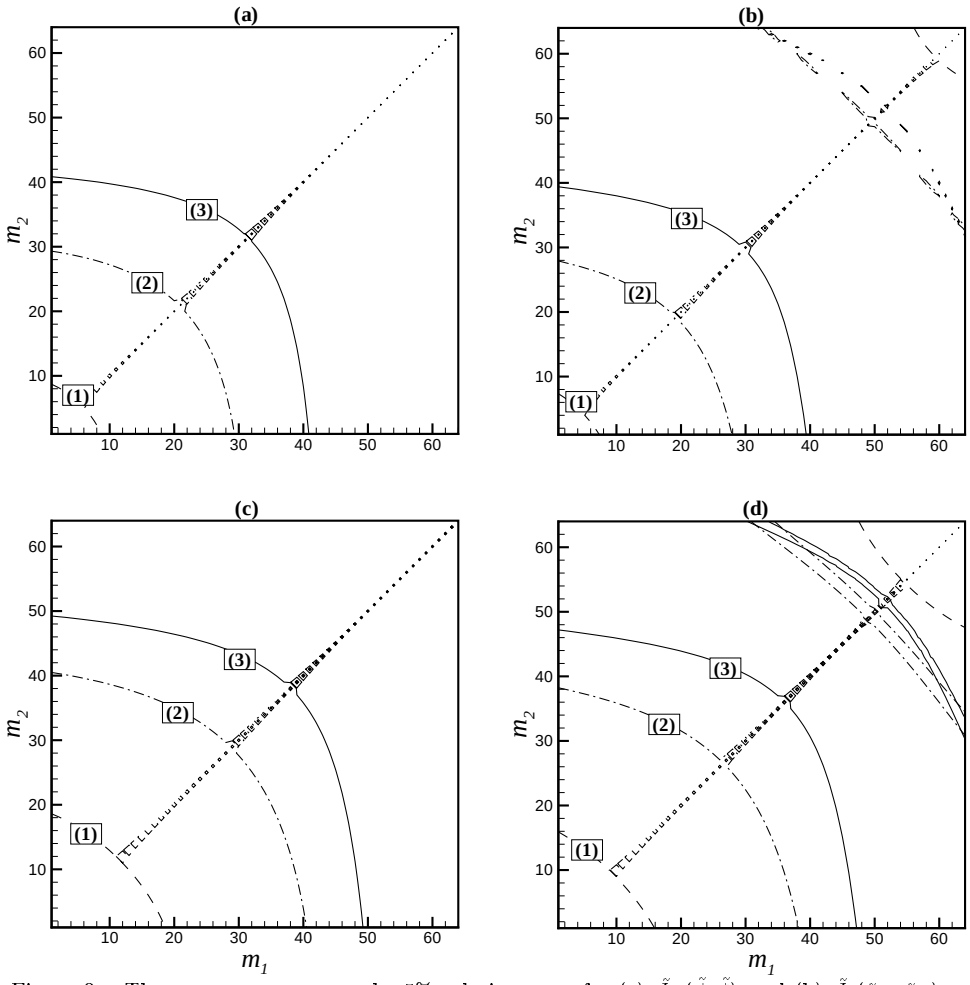

Figure 8. The contours represent the 5% relative error for (a) $\tilde{J}_{\mathrm{A}}(\tilde{\psi},\tilde{\zeta})$ and (b) $\tilde{J}_1(\tilde{u}_\psi,\tilde{v}_\psi)$, and the 20% relative error for (c) $\tilde{J}_{\mathrm{A}}(\tilde{\psi},\tilde{\zeta})$ and (d) $\tilde{J}_1(\tilde{u}_\psi,\tilde{v}_\psi)$. The dashed, dashed-dotted, and solid lines are for, respectively, (1) the second-order centred, (2) the fourth-order compact, and (3) the sixth-order SCFDM.

and the vorticity by

$$\zeta = 2\nu \sin\varphi - K \sin\varphi \cos^R \varphi (R^2 + 3R + 2) \cos R\lambda$$

where ν, K and R are constants as

$$\nu = K = 7.848 \times 10^{-6}\,\mathrm{s}^{-1}, \qquad R = 4$$

and $a = 6.37122 \times 10^6$ m is the radius of the Earth.

To find the streamfunction from the known vorticity field a Poisson equation on the sphere must be solved

$$\nabla^2 \psi = \zeta \tag{31}$$

where the Laplacian operator is

$$\nabla^2 = \frac{1}{a^2 \cos^2\varphi} \frac{\partial^2}{\partial\lambda^2} + \frac{1}{a^2 \cos\varphi} \left(\frac{\partial}{\partial\varphi} \cos\varphi \frac{\partial}{\partial\varphi} \right)$$

in which a is the Earth radius, λ the longitude and φ the latitude.

The Poisson equation is solved on a doubly periodic longitude-latitude grid system. The longitude-latitude grid system of Fornberg (1995) and Nihei and Ishii (2003) is used for the computation. The grid points in this system are arranged such that no grid points are at the poles. This grid system has the advantage of avoiding singularity at the poles and enabling the periodic boundary conditions to be imposed in both longitude and latitude directions. It should be noted that the sign of a quantity must be adjusted properly when using the periodic boundary condition in latitude direction, depending on whether the quantity is scalar or vector.

All of the three schemes are used to discretize the spatial derivatives of Eq. (31) to find the numerical streamfunction filed of the Rossby–Haurwitz wave. Spatial discretization of the derivatives are performed in both longitude and latitude directions which leads to solve a cyclic block tridiagonal system in each direction for the fourth-order compact and the sixth-order SCFDM and a cyclic tridiagonal system for the second order centred. These solutions are compared with the analytical streamfunction of the Rossby–Haurwitz wave to find the error of each scheme. The following normalised global error is used for the error measurement (Williamson *et al.* 1992):

$$l_2(q) = \frac{\left\{I\left(|q(\lambda,\varphi) - q_{\mathrm{E}}(\lambda,\varphi)|^2\right)\right\}^{1/2}}{\left\{I\left(|q_{\mathrm{E}}(\lambda,\varphi)|^2\right)\right\}^{1/2}} \tag{32}$$

where q and q_E are physical quantities of the numerical solution and the exact solution, respectively. The function I is defined as

$$I(q) = \frac{1}{4\pi}\sum_{k=1}^{N_\lambda}\sum_{l=1}^{N_\varphi} q_{k,l}\cos\varphi \cdot 2\sin(\Delta\varphi/2)\Delta\lambda \tag{33}$$

in which N_λ and N_φ are the number of grid points in longitude and latitude directions, $\Delta\lambda = 2\pi/N_\lambda$, $\Delta\varphi = \pi/N_\varphi$ and $q_{k,l}$ is a physical quantity at the grid point of $(\lambda_k, \varphi_l) = \{k\Delta\lambda, -\pi/2 + (l-1/2)\Delta\varphi\}$.

For periodic domains, ψ is known within a constant. It is meaningful to compare the accuracy of spatial derivatives of ψ entering into the computation of velocity components. Figure 9 shows the normalised global error l_2 for $\partial\psi/\partial\varphi$ at different horizontal resolutions in longitude and latitude directions, calculated for the second-order centred, fourth-order compact, and sixth-order SCFDM. It can be seen that the sixth-order SCFDM gives a marked improvement in accuracy on the fourth-order compact, almost the same as the improvement shown by the fourth-order compact on the scend-order centred. It is worth mentioning that the convergence rates shown by the three Poisson solutions are consistent with their order of accuracy. The higher accuracy exhibited by the fourth- and sixth-order Poisson solvers is essential for the long term performance of the vorticity (or potential vorticity)-divergence based primitive equation algorithms (Tolstykh 2002).

To compare the computational costs of the schemes, we have computed the CPU times for different resolutions. For example at 5 degrees resolution, the fourth-order compact method is 6 times more expensive than the second-order one and the sixth-order SCFDM is 2 times more expensive than the fourth-order compact method. It should be emphasized that the algorithms developed here to

solve the Poisson equation are not efficient and optimal solution procedures for every scheme can be devised. Furthermore, it is instructive to bring to attention the following issues. First, the extra cost of higher-order Poisson solvers can best be weighed against the higher accuracy achieved where they are used as part of a larger model like the shallow water equations. Second, when used only for latitudinal direction in combination with fast Fourier transform (FFT) in longitudinal direction the extra cost of the sixth-order SCFDM over the fourth-order compact (Tolstykh 2002) depends linearly on spatial resolution in latitudinal direction. On this count, a combined FFT-SCFDM algorithm seems feasible.

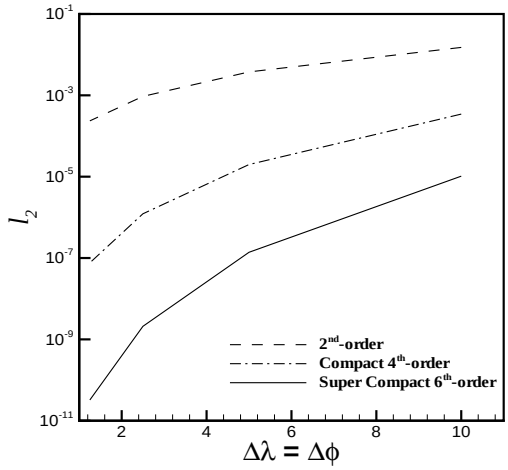

Figure 9. Normalised l_2 error of $\partial\psi/\partial\varphi$ field as a function of resolution obtained using the second-order centred, fourth-order compact, and sixth-order SCFDM for the Rossby–Haurwitz wave. A uniform resolution, shown in degrees in the figure, is used in both λ and φ directions.

6. Concluding remarks

For the linear propagation of inertia-gravity waves on the f-plane, the sixth-order SCFDM shows a significant improvement on the conventional second-order centred and the fourth-order compact. As a remark, we expect the same for the linear propagation of Rossby waves on the β-plane (Dukowicz 1995) and on the sphere. For the nonlinear problems represented by the Jacobians involved in vorticity advection by nondivergent flow and in Bolin–Charney balance equation, the improvement by the sixth-order SCFDM on the fourth-order compact in wavenumber distribution of the Jacobians is noticeable, amounting to nearly a 25% reduction in the global error measures presented. The higher accuracy is expected to manifest itself in both the long-term flow evolution and in maintaining nonlinear balance (see Mohebalhojeh and Dritschel 2000). For the reconstruction of the streamfunction of the vorticity field of the Rossby–Haurwitz wave, the sixth-order SCFDM improves markedly on the fourth-order compact. For all of the three problems considered, the second-order centred is manifestly in error.

What is certain is that the sixth-order SCFDM offers a promising finite-difference method to implement in idealised and real-world models of the atmosphere and oceans. It combines high accuracy over a great part of spectral space

with low cost and minimal stencil size. It involves only inverting block three-diagonal matrices whose computational cost depends linearly on spatial resolution. It enjoys a systematic derivation, which can be easily extended to higher orders.

The compact and super compact schemes can be implemented either fully or partially in models of the atmosphere in various ways. A full implementation (e.g. Spotz *et al.* 1998, Nihei and Ishii 2003) can be envisaged either in Eulerian flux/advective forms or in advective semi-Lagrangian algorithms of, for example, the shallow water equations. For Eulerian algorithms, the advantage of flux form to advective form is in the maintenance of global conservation of mass and vorticity, depending on formulation. A full implementation in flux form using potential vorticity, height, and divergence formulation is under way, where the issues of stability, dissipation, computational cost, and accuracy in complex, nonlinear flows involving wave–vortex interactions will be addressed. As partial implementation, we can refer to solving only the elliptic equations involved in various formulations of the shallow water equations, the simplest example of which is solving Poisson equations for streamfunction and velocity potential. Such application is also currently under way for the contour-advective semi-Lagrangian algorithms (Dritschel and Ambaum 1997, Dritschel *et al.* 1999) of the shallow water equations in spherical geometry.

Acknowledgements

Authors would like to thank University of Tehran and Atmospheric Science & Meteorological Research Centre (ASMERC) of Iran for support of this research.

References

Arakawa, A. and Lamb, R. 1977 Computational design of the basic dynamic processes of the UCLA general circulation model. *Methods in Computational Physics,* **17,** 174–265

Blayo, E. 2000 Compact finite difference schemes for ocean models 1. ocean waves. *J. Comput. Phys.,* **164,** 241–257

Chang, H. and Shirer, H. N. 1985 Compact spatial differencing techniques in numerical modeling. *Mon. Wea. Rev.,* **113,** 409–423

Dexun, Fu and Yanwen, Ma 1995 'High resolution schemes', Pp. 234–250 in *Computational Fluid Dynamic Review.* Ed. M. Hafez and K. Oshima, John Wiley & Sons.

Dexun, Fu and Yanwen, Ma 2001 Analysis of super compact finite difference method and application for simulation of vortex-shock interaction. *Inter. J. Numer. Meth. Fluids,* **36,** 773–805

Dritshel, D. G. and Ambaum, M. H. P. 1997 A contour-advective semi-Lagrangian algorithm for the simulation of fine-scale conservative fields. *Q. J. Roy. Meteorol. Soc.,***123,** 1097–1130

Dritschel, D. G., Polvani, L. M., and Mohebalhojeh, A. R. 1999 The contour-advective semi-Lagrangian algorithm for the shallow-water equations. *Mon. Wea. Rev.,* **127,** 1151–1165

Dukowicz, J. K. 1995 Mesh effects for Rossby waves. *J. Comput. Phys.,* **119,** 188–194

Esfahanian, V., Ghader, S. and Ashrafi, Kh. 2004 Accuracy analysis of super compact scheme in nonuniform grid with application to parabolized stability equations. *Inter. J. Numer. Meth. Fluids,* **46,** 485–505

Fornberg, B. 1995 A pseudospectral approach for polar and spherical geometries. *SIAM J. Sci. Comput.,* **16 (5),** 1071–1081

Ghader, S. 2000 'Numerical simulation of the stability of the laminar boundary layer flow over a flat plate by PSE equations using super compact method'. M.Sc. Thesis, University of Tehran

Haltiner, G. J. and Williams, R. T.	1980	*Numerical Prediction and Dynamic Meteorology.* 2nd ed, Wiley & Sons
Lilly, D. K.	1965	On the computational stability of numerical solutions of time-dependent nonlinear geophysical fluid dynamics problems. *Mon. Wea. Rev.*, **93**, 11–26
Lorenz, E. M.	1960	Maximum simplification of the dynamic equations. *Tellus*, **12**, 243–254
Mohebalhojeh, A. R. and Dritschel, D. G.	2000	On the representation of gravity waves in numerical models of the shallow water equations. *Q. J. Roy. Meteorol. Soc.*,**126**, 669–688
Nihei, T. and Ishii, K.	2003	A fast solver of the shallow water equations on a sphere using a combined compact difference scheme. *J. Comput. Phys.*, **187**, 639–659
Randall, D. A.	1994	Geostrophic adjustment and finite-difference shallow-water equations. *Mon. Wea. Rev.*, **122**, 1371-1377
Spotz, W. F., Taylor, M. A., and Swarztrauber, P. N.	1998	Fast shallow-water solvers in latitude-longitude coordinates. *J. Comput. Phys.*, **145**, 432–444
Tolstykh, M. A.	2002	Vorticity-divergence semi-Lagrangian shallow-water model of the sphere based on compact finite differences. *J. Comput. Phys.*, **179**, 180–200
Williamson, D. L., Drake, J. B., Hack, J. J., Jakob-Chien, R. and Swarztrauber, P. N.	1992	A standard test set for numerical approximations to the shallow water equations in spherical geometry. *J. Comput. Phys.*, **102**, 211–224
Yanwen, Ma and Dexun, Fu	1996	Super compact finite difference method (SCFDM) with arbitrary high accuracy. *Computational Fluid Dyn. J.*, **5(2)**, 259-276
Yuan, L., and Hamilton, K.	1994	Equilibrium dynamics in a forced-dissipative f-plane shallow-water system. *J. Fluid Mech.*, **280**, 369–394

Figure Captions

Figure 1: Definition of Arakawa's A-E grids and Randall's Z grid.

Figure 2: The exact and the sixth-order super compact representation of the nondimensional frequency $\omega/f_\circ$ for inertia-gravity waves with $\lambda/d = 2$. The horizontal coordinates in the plots are κd and ℓd, respectively, except for the E grid for which $\sqrt{2}\kappa d$ and $\sqrt{2}\ell d$ are used.

Figure 3: Contour lines of 10% error in frequency for the dispersion relationship of the inertia-gravity wave on A-E and Z grids obtained from the second-order method, (a) $\lambda/d = 2$ and (b) $\lambda/d = 1/2$.

Figure 4: Contour lines of 10% error in frequency for the dispersion relationship of the inertia-gravity wave on A-E and Z grids obtained from the fourth-order compact method, (a) $\lambda/d = 2$ and (b) $\lambda/d = 1/2$.

Figure 5: Contour lines of 10% error in frequency for the dispersion relationship of the inertia-gravity wave on A-E and Z grids obtained from the sixth-order super compact method, (a) $\lambda/d = 2$ and (b) $\lambda/d = 1/2$.

Figure 6: The potentio-vortical energy spectrum used to model the wavenumber distribution of the amplitude of ψ.

Figure 7: The distribution of exact values of (a) $J(\psi, \zeta)$ and (b) $J(u_\psi, v_\psi)$ obtained analytically from (26) and (27). The contours represent the amplitudes of the wave $(m_1 + m_2, 2n)$.

Figure 8: The contours represent the 5% relative error for (a) $\tilde{J}_{\mathrm{A}}(\tilde{\psi}, \tilde{\zeta})$ and (b) $\tilde{J}_1(\tilde{u}_\psi, \tilde{v}_\psi)$, and the 20% relative error for (c) $\tilde{J}_{\mathrm{A}}(\tilde{\psi}, \tilde{\zeta})$ and (d) $\tilde{J}_1(\tilde{u}_\psi, \tilde{v}_\psi)$. The dashed, dashed-dotted, and solid lines are for, respectively, (1) the second-order centred, (2) the fourth-order compact, and (3) the sixth-order SCFDM.

Figure 9: Normalised l_2 error of $\partial\psi/\partial\varphi$ field as a function of resolution obtained using the second-order centred, fourth-order compact, and sixth-order SCFDM for the Rossby–Haurwitz wave. A uniform resolution, shown in degrees in the figure, is used in both λ and φ directions.